J Mater Sci: Mater Electron (2015) 26:2205–2209
DOI 10.1007/s10854-015-2669-0

Structure and optical properties of $Zn_{0.99-x}Cd_xMn_{0.01}S$ quantum dots

Donglai Han · Jian Cao · Shuo Yang ·
Jinghai Yang · Qianyu Liu · Tingting Wang ·
Haifeng Niu

Received: 26 October 2014 / Accepted: 3 January 2015 / Published online: 13 January 2015

Abstract Wurtzite-type $Zn_{0.99-x}Cd_xMn_{0.01}S$ quantum dots (QDs) were synthesized facilely by the one-step solvothermal method. The as-prepared QDs had an average diameter of 4.0 ± 1.0 nm. The composition of the QDs was adjusted by controlling the Zn/Cd molar ratios. The successive shift of the XRD and PL patterns indicated that the QDs obtained were not a mixture of ZnS and CdS, but the $Zn_{1-x}Cd_xS$ solid solution. The red emission peak (coming from the cadmium vacancies), the yellow–orange emission peak (coming from the Mn^{2+} ions), and the green emission peak (coming from the intrinsic near band edge) were observed in the PL spectra, the intensity and position of which can be turned by controlling the Zn/Cd molar ratios effectively.

1 Introduction

Quantum dots (QDs) have attracted tremendous attention for their potential applications ranging from physics to medicine [1, 2]. Both ZnS and CdS are important direct band-gap semiconductors, which are considered important for applications such as ultraviolet-light-emitting diodes, electroluminescent devices, flat-panel displays, sensors and injection lasers [3]. As typical solid-solution semiconductors, ternary $Zn_{1-x}Cd_xS$ QDs are important in exploration of their continuously tunable optical properties for the desired wavelength through the gradual variation of their compositions, which often exhibits the improved structural and optical properties compared with their individual counterparts [4]. However, when the diameter of the QDs is <2 nm, the unstable optical property is inevitable [5]. In this regard, doping the transition metal ions into the $Zn_{1-x}Cd_xS$ QDs is presently a subject of immense interest to solve the problem [6]. Since that the doping ions can create the intermediate energy state between the valence band and conduction band of the QDs, change its photophysical relaxation process (such as lengthen the excited state lifetime), and improve the thermal stability [7]. It is well known that doping Mn^{2+} ions into the ZnCdS lattice can give rise to the strong yellow–orange light emission located at about 583 nm (through the $^4T_1$ to $^6A_1$ internal transition) with a high quantum yield (QY), the luminescence lifetime of which is about 1 ms [8]. Such a strong luminescence and long lifetime can make the light penetrate into and out of the tissues and distinguish the luminescence from the background autofluorescence.

Usually, the QDs were prepared by the organic phase growth method. It can produce the high quality QDs with good monodisperse and high PL QY, which usually require high temperature and hazardous organometallic precursors that have an adverse impact on the environment [9]. To date, researchers have not stopped trying to employ environmental friendly, simple, and low-cost methods in the fabrication of QDs. The aqueous synthesis has been proved

D. Han · S. Yang
Changchun Institute of Optics, Fine Mechanics and Physics,
Chinese Academy of Sciences, Changchun 130033, People's
Republic of China

D. Han · S. Yang
University of Chinese Academy of Sciences, Beijing 100049,
People's Republic of China

J. Cao (✉) · J. Yang (✉) · Q. Liu · T. Wang · H. Niu
Key Laboratory of Functional Materials Physics and Chemistry
of the Ministry of Education, Jilin Normal University,
Siping 136000, People's Republic of China
e-mail: caojian_928@163.com

J. Yang
e-mail: jhyang@jlnu.edu.cn

to be a simpler, cheaper, and less toxic method to prepare the water-soluble nanocrystals (NCs), however, usually suffered from some problems such as poor crystallinity and low PL QYs [10]. From the practical point of view, the solvothermal method requires a relatively low temperature, cheap precursors of low toxicity and makes easy for the introduction of the transition metal ions into the ZnCdS lattice [11]. In this paper, we firstly report the synthesis of the high-quality $Zn_{0.99-x}Cd_xMn_{0.01}S$ quaternary alloyed QDs with superior optical properties through one-step solvothermal method at 180 °C, and investigate their composition dependent structural and optical properties.

2 Experimental section

2.1 Preparation of products

In a typical process, 0.99−x mmol of zinc nitrate, x mmol of cadmium nitrate and 0.01 mmol manganese nitrate were dissolved in 16 ml ethanol and water (1:1 in volume ratio). Then stirring for 1 h, 3 mmol of thiourea were put into the resulting complex. After stirring for 2 h, the colloid solution was transferred into a 20-ml Teflon-lined autoclave and kept at 180 °C for 12 h. After the reaction, the autoclave was taken out and cooled down to room temperature. The product was washed with deionized water for several times and separated by centrifugation, and then dried at 80 °C for 1 h.

2.2 Characterization of products

X-ray diffraction (XRD) pattern was collected on a MAC Science MXP-18 X-ray diffractometer using a Cu target radiation source. High-resolution transmission electron microscopy (HRTEM) images were taken on JEM-2100 electron microscope. X-ray photoelectron spectrum (XPS) measurement was performed on a Vgescalab MK II X-ray photoelectron spectrometer (XPS) using Mg Kα radiation ($h\nu = 1253.6$ eV) with a resolution of 1.0 eV. Photoluminescence (PL) measurement was carried out at room temperature, using 325 nm as the excitation wavelength, He–Cd laser as the source of excitation.

3 Results and discussion

Figure 1 displays the XRD patterns of the $Zn_{0.99-x}Cd_xMn_{0.01}S$ NCs. It can be clearly seen that all the diffraction peaks of $Zn_{0.99}Mn_{0.01}S$ (x = 0) can be well indexed as the hexagonal wurtzite phase structure of ZnS, which are consistent with the standard card (JCPDS No. 36-1450). There is no extra diffraction peak from the doped Mn^{2+} ions for all the samples (Fig. 1) thereby suggesting that the Mn^{2+} ion have been incorporated into the ZnCdS lattice. As seen from $Zn_{0.09}Cd_{0.9}Mn_{0.01}S$ (x = 0.9), all the diffraction peaks can be well indexed as the hexagonal wurtzite phase structure of CdS, which are consistent with the standard card (JCPDS No. 41-1049). The structure conversion from the wurtzite ZnS (JCPDS No. 36-1450) to wurtzite CdS (JCPDS No. 41-1049) takes place as the Cd^{2+} doped ratio increased to 10 % (x = 0.1). As the Cd^{2+} doped ratio increased, all the diffraction peaks in the XRD patterns gradually shift to the lower angles. Such continuous reduction in 2θ indicates that the Cd^{2+} ions have gradually incorporated into the ZnS lattice or entered its interstitial sites, thus leading to the formation of the $Zn_{0.99-x}Cd_xMn_{0.01}S$ alloy solid solution. Since that the values in electronegativity of Cd (1.69) and Zn (1.65) are very close, which is favorable to form a solid solution alloy [12].

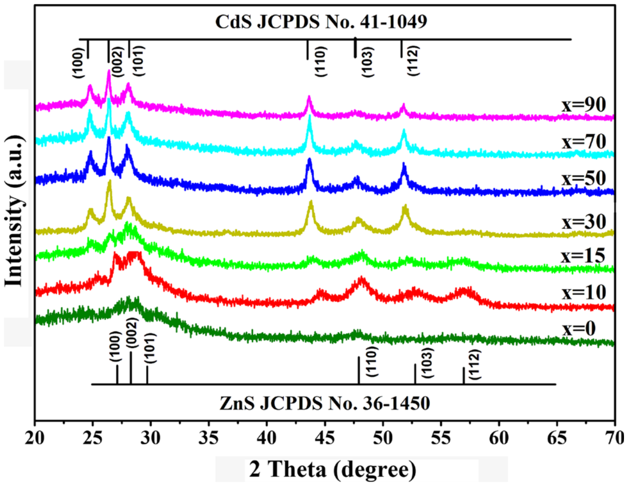

Fig. 1 XRD patterns of the $Zn_{0.99-x}Cd_xMn_{0.01}S$ NCs

Detailed microstructures of the as-prepared $Zn_{0.99-x}Cd_xMn_{0.01}S$ (x = 0.0, 0.1, 0.9) NCs were characterized by HRTEM. Figures 2a–c shows the HRTEM images of $Zn_{0.99}Mn_{0.01}S$, $Zn_{0.89}Cd_{0.1}Mn_{0.01}S$ and $Zn_{0.09}Cd_{0.9}Mn_{0.01}S$ NCs. It can be seen that the as-prepared NCs have an average diameter of 4.0 ± 1.0 nm, indicating the formation of the QDs. The displayed clear lattice spacing of 3.17 Å (Fig. 2a) is close to the lattice spacing of the (002) planes of the wurtzite ZnS ($d_{(002)} = 3.12$ Å for bulk wurtzite ZnS). The displayed clear lattice spacing of 3.37 Å (Fig. 2c) is in agreement with the lattice spacing of the (002) planes of the wurtzite CdS ($d_{(002)} = 3.36$ Å for bulk wurtzite CdS). So the lattice spacing of the (002) planes of the $Zn_{0.99-x}Cd_xMn_{0.01}S$ (x = 0.0, 0.1, 0.9) QDs is increased as the Cd^{2+} doped ratio increased. Since that the ionic radius of the Cd^{2+} ions (0.97 Å) is (31 %) larger than that of the Zn^{2+} ions (0.74 Å), the lattice expansion can be

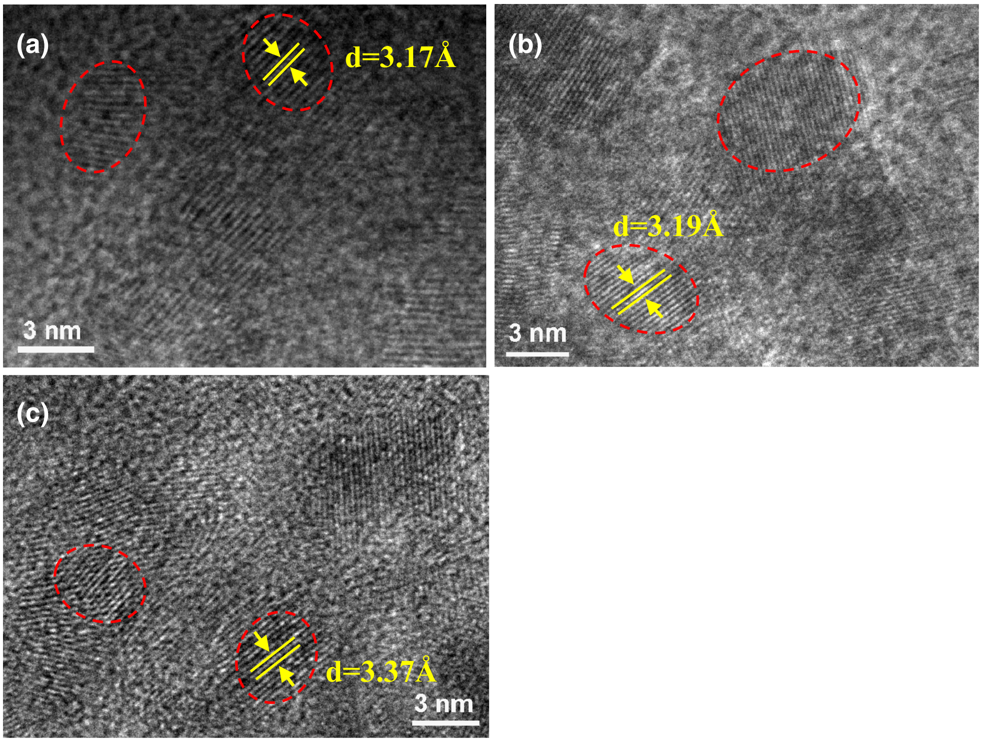

Fig. 2 HRTEM images of **a** $Zn_{0.99}Mn_{0.01}S$; **b** $Zn_{0.89}Cd_{0.10}Mn_{0.01}S$; **c** $Zn_{0.09}Cd_{0.90}$ $Mn_{0.01}S$ QDs

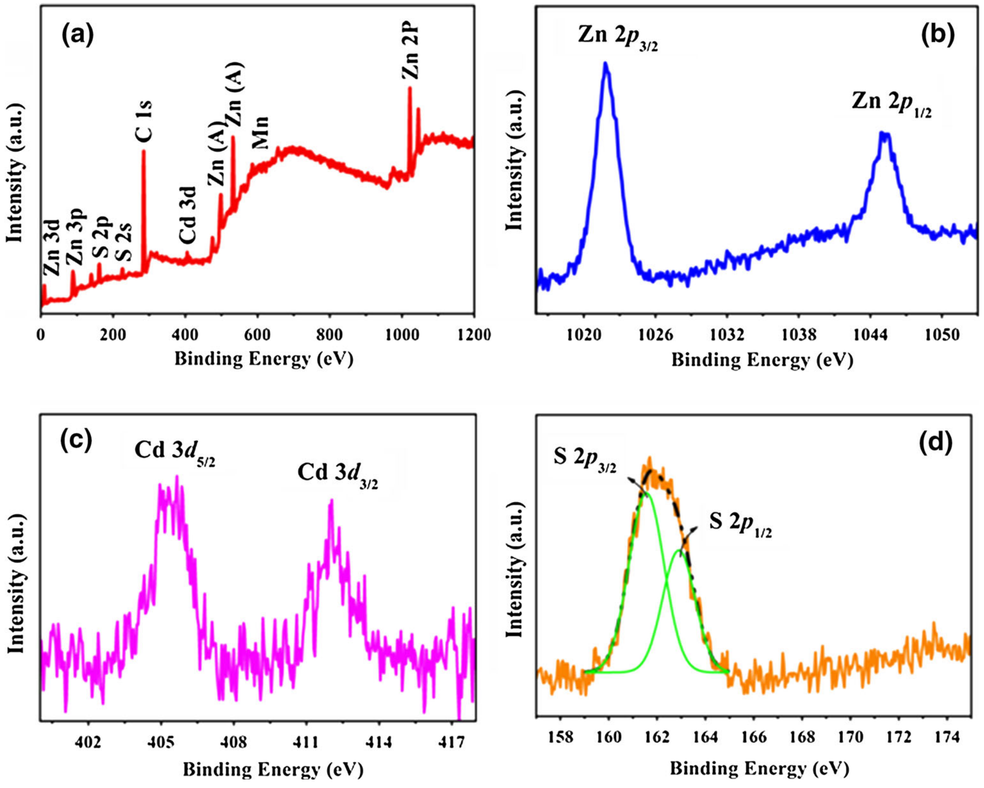

Fig. 3 **a** XPS survey spectrum of $Zn_{0.84}Cd_{0.15}Mn_{0.01}S$ QDs; **b**, **c**, **d** high-resolution binding energy spectrum of Zn 2*p*, Cd 3*d*, S 2*p* of the $Zn_{0.84}Cd_{0.15}Mn_{0.01}S$ QDs

Fig. 4 Room temperature PL spectra of $Zn_{0.99-x}Cd_xMn_{0.01}S$ QDs

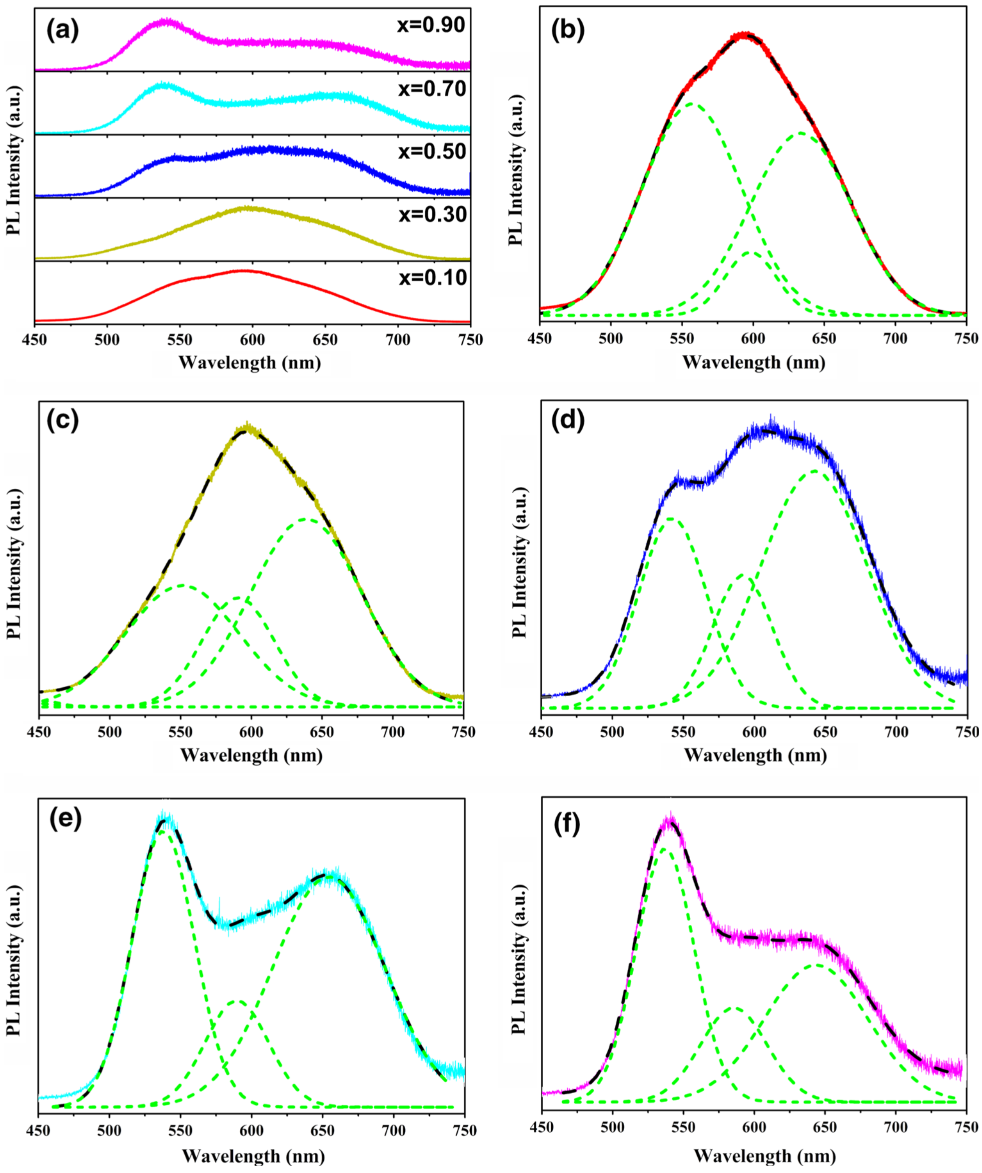

observed if the Cd^{2+} ions substituted for the Zn^{2+} sites in the $Zn_{0.99}Mn_{0.01}S$ QDs.

To investigate the surface information of the prepared samples, XPS analysis was carried out. Figure 3 is the typical XPS spectra of the as-prepared $Zn_{0.84}Cd_{0.15}Mn_{0.01}S$ QDs. The binding energy values obtained in the XPS analysis are corrected by referencing the C 1 s peak to 284.60 eV. The survey XPS spectrum (Fig. 3a) of the alloy QDs shows the presence of Zn, Cd, Mn and S. The presence of the carbon and oxygen in the survey spectrum is due to the carbon tape used for the measurement and the adsorbed gaseous molecules such as O_2, CO_2 and H_2O, respectively [13]. As shown in Fig. 3b, the high-resolution XPS spectrum of the Zn 2*p*3/2 peak in $Zn_{0.84}Cd_{0.15}Mn_{0.01}S$ QDs shows the peak at 1022.0 eV, corresponding to the Zn 2*p*3/2 peak of ZnS [14]. The high-resolution XPS spectrum of the Cd 3*d*5/2 peak (Fig. 3c) shows the peak centered at 405 eV, corresponding to the Cd 3*d*5/2 peak of CdS [15]. The high-resolution binding energy spectrum of the S 2*p* peak (Fig. 3d) can be decomposed into two Gaussian peaks. The peak centered at 161.6 and 162.9 eV is coming from the S 2*p*3/2 and S 2*p*1/2 peak of ZnS [16]. Since XPS does not usually detect Mn in doped ZnS nanostructure, as, the Mn peak is so weak comparable to the noise level.

Figure 4 shows the PL spectra of $Zn_{0.99-x}Cd_xMn_{0.01}S$ QDs at room temperature. As the Cd^{2+} doped ratio increased, the position of the emission peaks shows a systematically red shift from $Zn_{0.89}Cd_{0.1}Mn_{0.01}S$ to $Zn_{0.09}Cd_{0.9}Mn_{0.01}S$ QDs (Fig. 4a), which provide clear evidence for the formation of the alloyed $Zn_{1-x}Cd_xS$ QDs via intermixing the wider bandgap of ZnS (3.68 eV) with the narrower bandgap of CdS (2.48 eV), rather than forming separate ZnS, CdS or a core–shell structured NCs [17]. In Fig. 4b–f, it shows a broad emission band between 450 and 750 nm that can be decomposed into three Gaussian peaks. The broad red emission in the range of 633–654 nm is due to the extrinsic deep-level emission (DLE) which may originate from the non-stoichiometric defects, interstitial states, self-activated centers or impurities, but the most widely accepted reason for the origin of the red emission is the cadmium vacancies [18]. The yellow emission peak centered at around 590 nm is ascribed to the d–d ($^4T_1$–$^6A_1$) transition of the tetrahedrally coordinated Mn^{2+} states, indicating that the Mn^{2+} ions have been incorporated into the $Zn_{0.99-x}Cd_xMn_{0.01}S$ QDs [19]. For the $Zn_{0.09}Cd_{0.9}Mn_{0.01}S$ QDs (Fig. 4f), the strong green emission peak centered at 537.0 nm dominates the PL spectrum, which corresponds to the intrinsic near band edge (NBE) emission [20]. As the Cd^{2+} ions doped ratio increased, the intensity of the green emission peak is increased, the position of the green emission are blue shifted, which future prove that the synthesized samples are alloy solid solution and the optical properties can be turned by the controlling the compositions of the QDs effectively.

4 Conclusions

In this paper, the alloyed $Zn_{0.99-x}Cd_xMn_{0.01}S$ QDs were fabricated successfully by a one-step solvothermal method. The optical properties of the QDs were adjusted by controlling the Zn/Cd molar ratios. The formation of the solid solution QDs had been proved by the successive shift of the XRD and PL patterns. The red emission, yellow–orange emission and green emission were also observed. The intensity and position for these emission peaks can be turned by controlling the compositions of the QDs effectively.

Acknowledgment This work was financially supported by the National Programs for High Technology Research and Development of China (863) (Item No. 2013AA032202), the National Natural Science Foundation of China (Grant No. 61008051, 61178074, 11204104, 11254001, 61378085, 61308095).

References

1. I. Gur et al., Science **310**, 462–465 (2005)
2. G. Konstantatos et al., Naure **442**, 180–183 (2006)
3. M.Z. Wang et al., Appl. Phys. Lett. **103**, 213111–213115 (2013)
4. A.J. Waldau et al., Sol. Energy Mater. Sol. Cells **95**, 1509–1517 (2011)
5. Z. Qahtani et al., Mat. Sci. Semicond. Process. **20**, 68–73 (2014)
6. P.P. Ingole et al., J. Phys. Chem. C **117**, 7376–7383 (2013)
7. N.S. Karan et al., J. Phys. Chem. Lett. **1**, 2863–2866 (2010)
8. L. Liu et al., Chem. Phys. Lett. **539**, 112–117 (2012)
9. Z.X. Pan et al., ACS Nano **6**, 3982–3991 (2012)
10. R.M. Xing et al., Nanoscale **4**, 3135–3140 (2012)
11. H.Q. Huang et al., J. Lumin. **132**, 1003–1009 (2012)
12. S. Zu et al., J. Alloys Compd. **476**, 689–692 (2009)
13. S. Biswas et al., J. Phys. Chem. C **113**, 3617–3624 (2009)
14. G. Deroubaix et al., Surf. Interface Anal. **18**, 39–46 (1992)
15. D.S. Kim et al., J. Phys. Chem. C **111**, 10861–10868 (2007)
16. J.Y. Ji et al., J. Mater. Chem. **21**, 14498–14501 (2011)
17. Y. Chen et al., J. Phys. Chem. C **113**, 2263–2266 (2009)
18. Z. Yang et al., CrystEngComm **14**, 4298–4305 (2012)
19. J. Cao et al., J. Alloys Compd. **486**, 890–894 (2009)
20. G. Murali, et al. J. Alloys Compd. **581**, 849–855 (2013)